

Vector boson-tagged jet production in heavy ion collisions at the LHC

Zhong-Bo Kang,^{1,2,3,*} Ivan Vitev,^{3,†} and Hongxi Xing^{4,5,‡}

¹*Department of Physics and Astronomy, University of California, Los Angeles, California 90095, USA*

²*Mani L. Bhaumik Institute for Theoretical Physics,*

University of California, Los Angeles, California 90095, USA

³*Theoretical Division, Los Alamos National Laboratory, Los Alamos, New Mexico 87545, USA*

⁴*Department of Physics and Astronomy, Northwestern University, Evanston, Illinois 60208, USA*

⁵*High Energy Physics Division, Argonne National Laboratory, Argonne, Illinois 60439, USA*

(Dated: March 11, 2022)

Vector boson-tagged jet production in collisions of heavy nuclei opens new opportunities to study parton shower formation and propagation in strongly interacting matter. It has been argued to provide a golden channel that can constrain the energy loss of jets in the quark-gluon plasma created in heavy ion reactions. We present theoretical results for isolated photon-tagged and Z^0 boson-tagged jet production in Pb+Pb collisions with $\sqrt{s_{NN}} = 5.02$ TeV at the LHC. Specifically, we evaluate the transverse momentum imbalance x_{JV} distribution and nuclear modification factor I_{AA} of tagged jets and compare our theoretical calculations to recent experimental measurements by ATLAS and CMS collaborations. Our analysis, which includes both collisional and radiative energy losses, sheds light on their relative importance versus the strength of jet-medium interactions and helps quantify the amount of out-of-cone radiation of predominantly prompt quark-initiated jets.

I. INTRODUCTION

The production of a vector boson (either a photon γ or an electroweak boson such as the Z^0) in association with a jet has been extensively studied in proton-proton collisions at the Large Hadron Collider (LHC), by both the ATLAS [1–3] and CMS [4–7] collaborations. Such γ +jet and Z^0 +jet processes are among the most powerful channels that can be used to test the fundamental properties of Quantum Chromodynamics (QCD). They also serve as crucial inputs for the precise determination of the parton densities in the proton, and can help improve the constraints on the gluon distribution function. It is, thus, not surprising that significant theoretical effort has been invested in precisely computing the differential cross sections for these processes [8–10].

Vector boson-tagged jets are also particularly well suited to studying many-body QCD at high energies in heavy ion collisions, where a deconfined quark-gluon plasma (QGP) is expected to be formed. On one hand, the tagging bosons escape the region of the hot dense medium unscathed. This has been confirmed through the absence of significant modification of both γ and Z^0 boson production in Pb+Pb collisions relative to the binary collision-scaled proton-proton (p+p) baseline by both ATLAS and CMS collaborations [11–13]. On the other hand, the parton shower that recoils opposite the vector boson in heavy ion collisions gets modified, or quenched, due to the elastic and inelastic interactions with the QCD medium. Since at leading order the vector boson and the jet are produced back-to-back in the azimuthal plane and have equal transverse momenta in the standard collinear factorization framework, it was argued more than a decade ago [14] that a virtual photon that decays to dileptons ($\gamma^* \rightarrow \ell^+\ell^-$) will provide very tight constraints on the energy of the away-side parton shower. Theoretical studies of cold nuclear matter effects have shown that they don't significantly affect vector boson-tagged jet distributions [15].

However, only recently have measurements of approximately back-to-back isolated γ +jet and/or Z^0 +jet¹ final states, considered “golden channels” for the study of jet quenching and the extraction of the properties of the hot dense medium, become possible. It was also realized that higher order processes will alter the perfect transverse momentum balance $p_T^J = p_T^V$ and lead to a distribution of recoiling jets [17]. A useful feature of this distribution for the purpose of our study is that it is narrowly peaked and the shift of the peak will contain detailed information about jet energy loss. Furthermore, jets produced opposite to the isolated γ or Z^0 bosons are much more likely to originate from quarks, while dijets usually involve significant quark and gluon fractions that vary strongly with transverse momentum. In this regard, vector boson-tagged jets can help constrain the flavor dependence of the jet quenching mechanism. Previous studies of vector boson tagged jet production in heavy ion collisions have been carried out based on a perturbative QCD framework [15, 18], a Boltzmann transport model [19], an event generator JEWEL [20],

* zkang@physics.ucla.edu

† ivitev@lanl.gov

‡ hxing@northwestern.edu

¹ The so-called fragmentation contribution to Z^0 -boson production is generally small even at the LHC energies [16].

and a hybrid strong/weak coupling model [21]. Photon-tagged heavy flavor jets have also been proposed as ways to increase the fraction of prompt b quarks [22]. Last but not least, the substructure of γ -tagged jets was found to be more sensitive to large angle radiation in comparison to inclusive jets [23].

Isolated γ -tagged and Z^0 -tagged jets in Pb+Pb collisions at the center-of-mass energy per nucleon pair $\sqrt{s_{NN}} = 5.02$ TeV have been recently measured at the LHC by the ATLAS and CMS collaborations [24–26]. Motivated by these new measurements, in this paper, we provide our theoretical calculations and comparison to the experimental data. In particular, by including both collisional and radiative energy loss effects, we evaluate the so-called transverse momentum imbalance x_{JV} distribution in both p+p and Pb+Pb collisions, where $x_{JV} = p_T^J/p_T^V$ with p_T^J and p_T^V the transverse momentum of the jet and the vector boson, respectively. We also calculate the nuclear modification factor I_{AA} and compare to the experimental findings. Within the theoretical model calculation we present our results for the transverse momentum imbalance shift $\Delta\langle x_{JV} \rangle$ and the relative contribution of radiative and collisional energy losses of typical energy jets.

The rest of our paper is organized as follows. In Sec. II, we present the evaluation of the differential cross sections for isolated γ -tagged and Z^0 -tagged jet production in p+p collisions using Pythia 8 [27] and determine the flavor origin of the recoil jet production for the proper implementation of the energy loss effects. In Sec. III, we provide information on how we implement the medium effects to obtain the modification of vector boson tagged jet production in dense QCD matter. In Sec. IV, we present our phenomenological results and give detailed comparison with the most recent experimental measurements for the isolated γ and Z^0 boson tagged jet production in heavy ion collisions at the LHC. We summarize our paper in Sec. V.

II. ISOLATED PHOTON-TAGGED AND Z^0 -TAGGED JET PRODUCTION IN P+P COLLISIONS

In this section we present the evaluation of the differential cross sections for isolated photon-tagged and Z^0 -tagged jet production in p+p collisions using Pythia 8 [27]. Pythia 8 is a widely-used high energy phenomenology event generator, which can describe well the main properties of the event structure. This event generator utilizes leading-order perturbative QCD matrix elements+parton shower, combined with the Lund string model for hadronization. The simulations presented in this paper are performed with the CTEQ6L1 parton distribution functions [28] and with the anti- k_T jet clustering algorithm [29]. In the p+p baseline simulations, we select the vector boson (isolated-photon and Z^0 -boson) and jet according to the desired kinematics to match the experimental measurements, and we have simulated around 10^7 events for both isolated photon-tagged and Z^0 -tagged jets to reduce the statistical uncertainties/fluctuations.

Measurements of vector boson-tagged jet production in p+p collisions at different center-of-mass energies have been carried out at both the Tevatron and the LHC. We present in Fig. 1 the comparisons to CMS measurements [6, 7] to show the validation of Pythia simulation against experimental data. The left panel in Fig. 1 is the differential cross section $d\sigma/dp_T^J$ as a function of leading jet transverse momentum p_T^J for Z^0 +jet production in p+p collisions at the LHC at $\sqrt{s} = 7$ TeV. The right panel corresponds to the differential cross section $d\sigma/dp_T^\gamma$ as a function of isolated-photon transverse momentum p_T^γ for γ +jet production in p+p collisions at the LHC at $\sqrt{s} = 8$ TeV. In our simulations, the specific kinematic requirements are implemented to match the experimental measurements in selecting V+jet events. For details on the kinematic cuts, see Ref. [6] for Z^0 +jet and Ref. [7] for γ +jet production. As can be seen in Fig. 1, the Pythia 8 event generator gives reasonably good description of the CMS experimental data.

Before the implementation of energy loss effects through the medium-induced parton shower on vector boson-tagged jet production in Pb+Pb collisions at the LHC, we need the detailed baseline information for Z^0 +jet and γ +jet production in p+p collisions for different partonic subprocesses. In our simulations, specific kinematic cuts for the Z^0 +jet and γ +jet event selections are applied as in Refs. [24] and [25], respectively. In particular, a minimum separation of the azimuthal angle between the vector boson and the jet, $\Delta\phi_{JV} > 7/8\pi$, is required to select back-to-back V+jet events. In each event of the Z^0 +jet simulation, the Z^0 -boson is required to have: the invariant mass of the decayed dileptons $70 < m_{\ell\ell} < 110$ GeV, $p_T^e > 20$ GeV, $p_T^\mu > 10$ GeV, $|y^e| < 2.5$, $|y^\mu| < 2.4$, and the transverse momentum of the Z^0 boson $p_T^{Z^0} > 60$ GeV; the recoil jet is reconstructed using the anti- k_T algorithm with a jet radius parameter $R = 0.3$, $p_T^J > 30$ GeV and $|y|^J < 1.6$ in the same event. For γ +jet production, the photon is required to have $|y^\gamma| < 1.44$. To minimize the fragmentation contribution to the photon, an isolation cut is applied where the sum of the transverse momenta of the generated particles in a cone of radius $\Delta R = 0.4$ around the photon is required to be less than 5 GeV. Unless explicitly specified, these kinematical cuts apply to all the results shown in the rest of the paper.

In V+jet production, there are two dominant channels at leading order that are implemented in Pythia, i.e. $q + \bar{q} \rightarrow V + g$ and $q(\bar{q}) + g \rightarrow V + q(\bar{q})$. We have checked that the $g + g \rightarrow V + g$ channel contributes to the cross section only marginally and, thus, can be safely neglected. As can be seen in Fig. 2 (left), the cross section of Z^0 +jet

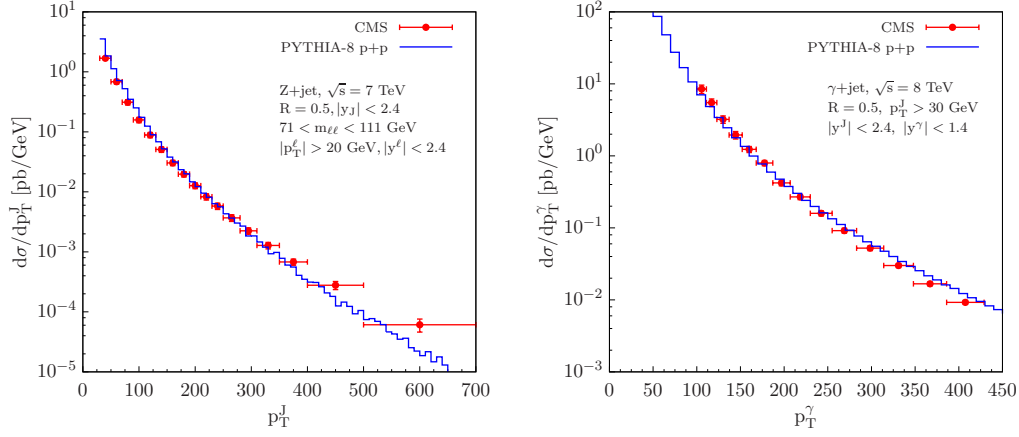


FIG. 1. Comparison between Pythia 8 simulations and CMS measurements of V+jet production in p+p collisions at the LHC. Left: the Z^0 +jet differential cross section at $\sqrt{s} = 7$ TeV as a function of p_T^J . Right: the isolated photon+jet differential cross section at $\sqrt{s} = 8$ TeV as a function of p_T^γ . The blue curves are from Pythia 8 simulations, the red data points are from the CMS collaboration [6, 7].

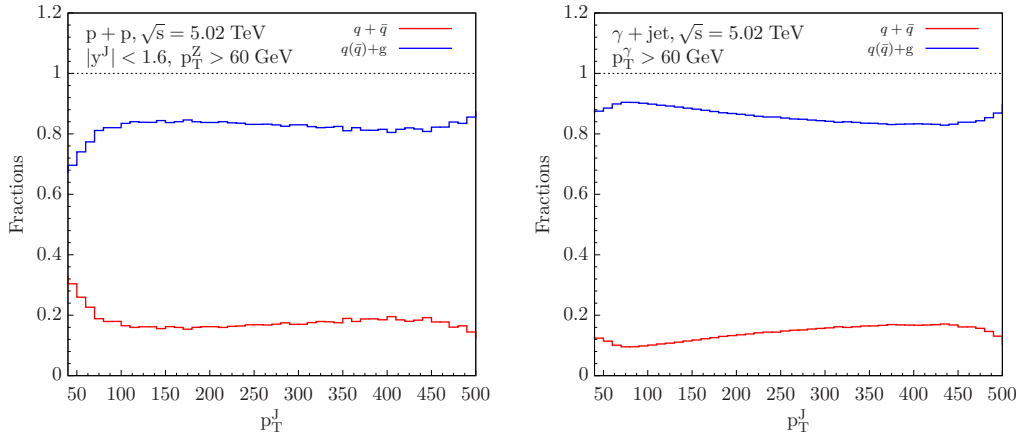


FIG. 2. The fractional contributions of different subprocesses to the Z^0 +jet (left) and isolated- γ +jet (right) production cross sections in p+p collisions at $\sqrt{s} = 5.02$ TeV. Kinematical cuts are implemented in our simulations as in CMS measurements, see Ref. [30] for Z^0 +jet and Ref. [25] for isolated- γ +jet.

production is dominated by $q(\bar{q}) + g \rightarrow Z + q(\bar{q})$ channel (around 80%) for a wide p_T range. In other words, the produced jet predominantly originates from a light quark. The fraction for γ +jet production behaves similarly to the case of Z^0 +jet production, with even higher fractions from the $q(\bar{q}) + g \rightarrow \gamma + q(\bar{q})$ channel. This implies that in heavy ion collisions at LHC energies, the medium modification of V+jet production is dominated by quark energy loss. We will present the detailed discussions about the medium effects on V+jet production in the next section.

III. MODIFICATION OF TAGGED JET PRODUCTION IN DENSE QCD MATTER

In the presence of dense QCD matter, such as the QGP created in heavy-ion collisions, the vacuum parton shower is modified. Early investigations focused on non-Abelian energy loss processes [31–36]. The soft gluon emission limit was subsequently relaxed to allow for a unified description of parton branching processes [37, 38]. In addition to radiative processes, collisional energy loss has also attracted a lot of attention [39–44] and was found to play a more significant role for lower parton energies.

At present, the application of full in-medium splitting functions [45, 46] has not been combined with collisional energy loss processes. For this reason, we here follow the soft gluon emission radiative energy loss approximation. The benefit of this approach is that it allows us to consider multiple emissions. For a given impact parameter $|\mathbf{b}_\perp|$,

taken along the x -axis in the transverse plane of nucleus-nucleus collisions, we evaluate the cross sections as follows

$$\begin{aligned} \frac{d\sigma^{AA}(|\mathbf{b}_\perp|)}{dp_T^V dp_T^J} &= \int d^2\mathbf{s}_\perp T_A\left(\mathbf{s}_\perp - \frac{\mathbf{b}_\perp}{2}\right) T_A\left(\mathbf{s}_\perp + \frac{\mathbf{b}_\perp}{2}\right) \sum_{q,g} \int_0^1 d\epsilon \frac{P_{q,g}(\epsilon; s_\perp, |\mathbf{b}_\perp|)}{1 - f_{q,g}^{\text{loss}}(R; s_\perp, |\mathbf{b}_\perp|) \epsilon} \\ &\times \frac{d\sigma_{q,g}^{NN}(p_T^V, p_T^J / \{1 - f_{q,g}^{\text{loss}}(R; s_\perp, |\mathbf{b}_\perp|) \epsilon\})}{dp_T^J dp_T^V}, \end{aligned} \quad (1)$$

Let us now discuss Eq. (1). Hard processes in heavy ion collisions follow a binary collision density distribution in the transverse plane at position \mathbf{s}_\perp . This means that the point-like large Q^2 scattering is distributed $\propto T_A(\mathbf{s}_\perp - \mathbf{b}_\perp/2) T_A(\mathbf{s}_\perp + \mathbf{b}_\perp/2)$, where $T_A(\mathbf{s}_\perp) = \int_{-\infty}^{\infty} \rho_A(\mathbf{s}_\perp, z) dz$. In our calculation we use an optical Glauber model and inelastic nucleon-nucleon scattering cross sections $\sigma_{\text{in}} = 70$ mb to obtain average number of binary collisions at $\sqrt{s_{NN}} = 5.02$ TeV.

In heavy ion collisions a fraction ϵ of the energy of the parent parton can be redistributed through medium-induced bremsstrahlung. This process is independent on whether a jet is reconstructed or not, but reflects instead the parton energy, color charge, path length and medium properties dependence of the non-Abelian bremsstrahlung. The probability distribution $P_{q,g}(\epsilon)$ of this energy fraction satisfies the following properties

$$\int_0^1 P_{q,g}(\epsilon) d\epsilon = 1, \quad \int_0^1 \epsilon P_{q,g}(\epsilon) d\epsilon = \frac{\langle \Delta E_{q,g}^{\text{rad}} \rangle}{E_{q,g}}, \quad (2)$$

for every jet energy and every transverse position \mathbf{s}_\perp at a given impact parameter. To calculate this probability, we first need to evaluate the medium-induced gluon radiative spectrum

$$\begin{aligned} \frac{dN_{q,g}^g(\omega, r)}{d\omega dr} &\propto C_R \alpha_s \int_0^\infty d\Delta z \frac{1}{\lambda_g(\Delta z)} \left[\int d^2\mathbf{q} \left(\frac{1}{\sigma_{el}(\Delta z)} \frac{d\sigma_{el}(\Delta z)}{d^2\mathbf{q}} - \delta^2(\mathbf{q}) \right) \right] \\ &\times \frac{2\mathbf{k} \cdot \mathbf{q}}{\mathbf{k}^2(\mathbf{k} - \mathbf{q})^2} \left\{ 1 - \cos \left[\frac{(\mathbf{k} - \mathbf{q})^2 \Delta z}{2\omega} \right] \right\} \end{aligned} \quad (3)$$

of parent quarks and gluons. Here, ω and r are the energy and angle of the radiated gluon and for small angles $|\mathbf{k}| = \omega r$. This calculation is performed to first order in opacity and the integral over Δz is along the path of the jet propagation through the QGP medium from the hard collision point. In the soft gluon emission limit only the gluon scattering length λ_g plays a role and quarks and gluons lose energy strictly proportional to their squared color charge. The Casimir C_R in Eq. (3) is $C_F = 4/3$ for parent quarks and $C_A = 3$ for parent gluons. The momentum transfers \mathbf{q} between the jet and the medium are distributed according to a normalized differential elastic scattering cross section, including a unitarizing forward scattering contribution.

The spectrum is first averaged over the collision geometry, see for example the first line of Eq. (1). In the QGP we include an effective gluon mass via $\mathbf{k}^2 \rightarrow \mathbf{k}^2 + \mu_D^2(\Delta z)$. In this evaluation the exact leading power and sub-leading logarithmic dependence in the path length, density and coupling g between the jet and the medium is retained. In the gluon emission vertex the strong coupling is taken to run with the transverse gluon mass. In the application of Eq. (1) the point-by-point in collision geometry radiative gluon spectrum is unfolded to leading power in the path length, coupling g and gluon density, which goes as $\propto g^4 \int d\Delta z \Delta z \rho_g(\mathbf{s}_\perp + \mathbf{n}_\perp \Delta z, \tau_0 + \Delta z)$. Here \mathbf{n} is the direction of jet propagation and we take the medium formation time $\tau_0 = 0.3$ fm. On a position-by-position basis and for every parent parton energy E we can then obtain

$$\frac{dN_{q,g}^g(\omega)}{d\omega} = \int_0^{R_{\text{max}}} dr \frac{dN^g(\omega, r)}{d\omega dr}, \quad \langle N_{q,g}^g \rangle = \int_0^E d\omega \frac{dN^g(\omega)}{d\omega}. \quad (4)$$

In Eq. (4) $R_{\text{max}} \gg 1 > R$ is a large radius chosen to capture the parton shower. In our calculation we use $R_{\text{max}} = 2$. In the Poisson approximation the probability density for fractional energy loss $\epsilon = \sum_i \omega_i / E$ can be obtained as follows

$$P_{q,g}(\epsilon) = \sum_{n=0}^{\infty} P_{q,g}^n(\epsilon), \quad P_{q,g}^0(\epsilon) = e^{-\langle N_{q,g}^g \rangle} \delta(\epsilon), \quad P_{q,g}^{n+1}(\epsilon) = \frac{1}{n+1} \int_0^E d\omega \frac{dN_{q,g}^g(\omega)}{d\omega} P_{q,g}^n\left(\epsilon - \frac{\omega}{E}\right). \quad (5)$$

For inclusive and tagged hadron production, unless one focuses on the p_T region below 5 GeV, the fragmentation of radiated gluons does not contribute because they are typically soft. Since jets are defined by the amount of energy reconstructed inside the jet cone of radius parameter R , the evaluation of cross sections with jets in the final state critically depends on the determination of how much of the energy of the medium-induced parton shower actually falls

outside of the jet [47]. We here denote this fraction by $f_{q,g}^{\text{loss}}(R)$, suppressing all other dependencies of this quantity. Let us first concentrate only on radiative processes. In this case we have

$$f_{q,g}^{\text{loss}}(R; \text{rad}) = \left(\int_R^{R_{\text{max}}} dr \int_0^E d\omega \frac{dN_{q,g}^g(\omega, r)}{d\omega dr} \right) / \left(\int_0^{R_{\text{max}}} dr \int_0^E d\omega \frac{dN_{q,g}^g(\omega, r)}{d\omega dr} \right). \quad (6)$$

The radiative out-of-cone energy loss is purely determined by the wide-angle medium-induced radiation pattern.

Collisional interactions take energy away from the jet through the excitation of the QGP medium and dissipation of the energy away from the collision axis. The amplification of the collisional energy loss effects comes from the multiple emitted gluons [48]. In our simulation we assume that all of the energy is taken away from the jet. This is justified because we consider jets of small radius $R \ll 1$, whereas Mach cones shockwaves propagate at angles $\theta_M = \arcsin c_s$. Thus, taking $c_s \approx 1/3$, we find $\theta_M \sim 1$ and the energy deposited by collisional processes is transported out of the jet cone. It is important to realize that considering radiative energy loss only and radiative+collisional energy loss of the type discussed here covers the two extreme possible cases. If part of the energy is not fully dissipated, this will be a situation that falls in-between those two scenarios. From the average gluon number and the mean total radiative energy loss we can determine the mean energy per emitted gluon $\langle \omega_{q,g} \rangle = \langle \Delta E_{q,g} \rangle / \langle N_{q,g}^g \rangle$. Parametrically, the collisional energy loss rate to leading logarithmic accuracy goes as $d\Delta E^{\text{coll}}/d\Delta z \propto C_R g^2 \mu_D^2 \ln(E/\mu_D)$. In Ref. [48] we set a simulation of the collisional energy loss of the medium-induced shower as the parent parton propagates through the medium and showers off gluons. The average number of gluons, rounded to an integer number, were distributed along the path of jet propagation at positions z_i and the net collisional energy loss obtained. Since the softer medium-induced gluons thermalize first, for later convenience we can express this total collisional energy loss as an integral over the spectrum of the medium induced gluons

$$\Delta E_{q,g}^{\text{coll}}(\text{tot.}) = \sum_{i=1}^{N_{q,g}^{\text{tot. partons}}} \int_{z_i}^{\infty} \frac{d\Delta E_i^{\text{coll}}}{d\Delta z} d\Delta z, \quad \Delta E_{q,g}^{\text{coll}}(\text{tot.}) = \int_0^{\omega_{\text{min}}} d\omega \int_0^{R_{\text{max}}} dr \omega \frac{dN_{q,g}^g(\omega, r)}{d\omega dr}. \quad (7)$$

The collisional energy loss that Eq. (7) refers to is the one of the full medium induced parton shower. From the perspective of reconstructed jets, however, only the collisional energy loss of the medium-induced parton shower that falls inside the jet cone of radius R will modify the observed cross sections. Thus, when collisional energy losses are included the out-of-cone energy fraction of the medium-induced shower is

$$f_{q,g}^{\text{loss}}(R; \text{rad} + \text{coll}) = 1 - \left(\int_0^R dr \int_{\omega_{\text{min}}}^E d\omega \frac{dN_{q,g}^g(\omega, r)}{d\omega dr} \right) / \left(\int_0^{R_{\text{max}}} dr \int_0^E d\omega \frac{dN_{q,g}^g(\omega, r)}{d\omega dr} \right). \quad (8)$$

Clearly, the expression above reduces to Eq. (6) when $\omega_{\text{min}} = 0$. This concludes the discussion of Eq. (1).

IV. PHENOMENOLOGICAL RESULTS

In this section we present our phenomenological results and provide detailed comparison with the most recent experimental measurements for the isolated γ -tagged and Z^0 boson-tagged jet production in Pb+Pb collisions at $\sqrt{s_{NN}} = 5.02$ TeV at the LHC.

In the absence of in-medium interactions one expects, to leading order in perturbative QCD, that the transverse momentum of the vector boson is balanced by the transverse momentum of the jet, $p_T^V = p_T^J$. Next-to-leading order processes, and the development of parton showers in general, break this equality. Jet reconstruction algorithms, jet radius reconstruction choice, experimental cuts, and detector resolution effects can all affect the exact differential distribution of $d\sigma/dp_T^V dp_T^J$. Still, the downshift of this distribution to smaller values of p_T^J in general or the downshift of the peak in $x_{JV} = p_T^J/p_T^V$ space are currently the best proxies for jet energy loss. This so-called transverse momentum imbalance x_{JV} distribution can be obtained from the double differential distribution of V+jet cross section

$$\frac{d\sigma}{dx_{JV}} = \int_{p_T^{J,\text{min}}}^{p_T^{J,\text{max}}} dp_T^J \frac{p_T^J}{x_{JV}^2} \frac{d\sigma(p_T^V = p_T^J/x_{JV}, p_T^J)}{dp_T^V dp_T^J}, \quad (9)$$

where $p_T^{J,\text{min}}$ and $p_T^{J,\text{max}}$ are matched to the desired cuts of the experimental measurements.

In Fig. 3 we plot the normalized momentum imbalance distributions for the Z^0 +jet channel (normalized by the Z^0 boson cross section) in both p+p and Pb+Pb collisions at the LHC, and compare the calculations to the CMS measurements [24]. Here, the black dashed histogram shows the Pythia 8 simulation for the p+p baseline, and the

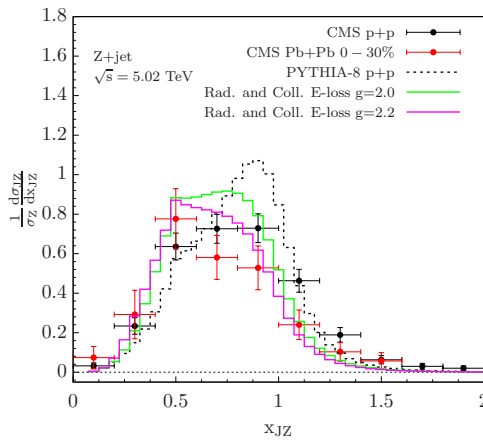


FIG. 3. The Z^0 -tagged jet asymmetry distribution at $\sqrt{s} = 5.02$ TeV in p+p (black) and Pb+Pb (red) collisions at the LHC. The jet radius parameter is $R = 0.3$, and the transverse momenta of the Z^0 boson and the jet are $p_T^Z > 60$ GeV and $p_T^J > 30$ GeV, respectively. The p+p baseline is simulated by Pythia 8 and shown by the black dashed line. The theoretical results for Pb+Pb collisions with two different jet-medium coupling strength are shown by the green ($g = 2.0$) and magenta ($g = 2.2$) histograms. The data is from the CMS collaboration [24].

black solid points represent the CMS results. One can see that the x_{JV} distribution from Pythia 8 simulation is narrower than the one measured by the CMS experiment for the p+p reference. We anticipate that this is mainly due to detector resolution effects that have not been unfolded in the data analysis². The results of our theoretical calculations in Pb+Pb collisions are shown in green and magenta histograms, which correspond to jet-medium coupling strengths $g = 2.0$ and $g = 2.2$, respectively. These values have worked well in describing the single inclusive hadron [49, 50], heavy flavor mesons [51], and jet suppression data [46] at the LHC. In the implementation of energy loss effects, we have included both medium-induced radiative energy loss and energy dissipation of parton showers through collisional interactions between the jet and the medium, detailed description of these two energy loss effects can be found in the last section. By comparing Pb+Pb to p+p results, one can clearly see the downshift of x_{JV} , as shown in Fig. 3, which agrees with the data quantitatively in terms of the difference between p+p and Pb+Pb. This downshift can be easily explained by the nature of energy loss effects. The Z^0 -boson escapes out of the medium unscathed, while part of the energy of away-side parton shower is redistributed outside of the jet cone. This reduces the jet transverse momentum and results in the downshift of the x_{JV} distribution in Pb+Pb collisions.

To further quantify the downshift of the x_{JV} distribution, we define the mean value of x_{JV} ,

$$\langle x_{JV} \rangle = \left(\int dx_{JV} x_{JV} \frac{d\sigma}{dx_{JV}} \right) / \left(\int dx_{JV} \frac{d\sigma}{dx_{JV}} \right). \quad (10)$$

In Table I we show the difference for $\langle x_{JV} \rangle$ in p+p and Pb+Pb collisions, i.e.,

$$\Delta \langle x_{JV} \rangle = \langle x_{JV} \rangle_{pp} - \langle x_{JV} \rangle_{PbPb}. \quad (11)$$

The positive values of $\Delta \langle x_{JV} \rangle$ represent downshifts of the x_{JV} distribution, and they are consistent with the experimental data within the measurement uncertainties for different p_T^Z cuts. From our theoretical results, we can see the p_T^Z cut dependence of $\Delta \langle x_{JV} \rangle$, it gets larger with the increase of p_T^Z cut. However, this can't be clearly identified within the current experimental error bars.

We also evaluated the cross section for isolated- γ -tagged jet production in p+p and Pb+Pb collisions at the LHC. The comparisons to CMS and ATLAS measurements are shown in Figs. 4 and 5, respectively. Notice that the recoil jet is reconstructed with the anti- k_T algorithm with $R = 0.4$ (0.3) at ATLAS (CMS). We have considered both central collisions (0–10%) and semi-central (30–50%) collisions. In general, theoretical calculations of the difference between $x_{J\gamma}$ distributions in p+p and Pb+Pb are quite compatible with what is seen in experimental data. One exception is that we didn't see as significant nuclear modifications in semi-central (30–50%) collisions as present in the ATLAS measurements in Fig. 5 (right). We have also computed $\Delta \langle x_{J\gamma} \rangle$ and the numerical values are given in Table II for

² By applying the same smearing functions, as those that experiments apply to Monte Carlo simulations, to our calculated 3-D p_T distributions for p+p and Pb+Pb collisions, we expect to get broader x_{JZ} distributions which would bring the curves for both p+p and Pb+Pb closer to the data points.

TABLE I. Theoretical results for the difference of the average x_{JZ} between p+p and Pb+Pb central collisions (0 – 30%). The center of mass energy is $\sqrt{s} = 5.02$ TeV, the transverse momentum cut for the recoil jet is $p_T^J > 30$ GeV.

p_T^Z (GeV)	$\Delta\langle x_{JZ} \rangle$			
	40 – 50	50 – 60	60 – 80	80 – 120
CMS [24]	0.061 ± 0.059	0.123 ± 0.051	0.124 ± 0.052	0.068 ± 0.042
Rad. + Coll. $g = 2.0$	0.022	0.050	0.075	0.086
Rad. + Coll. $g = 2.2$	0.024	0.058	0.093	0.119

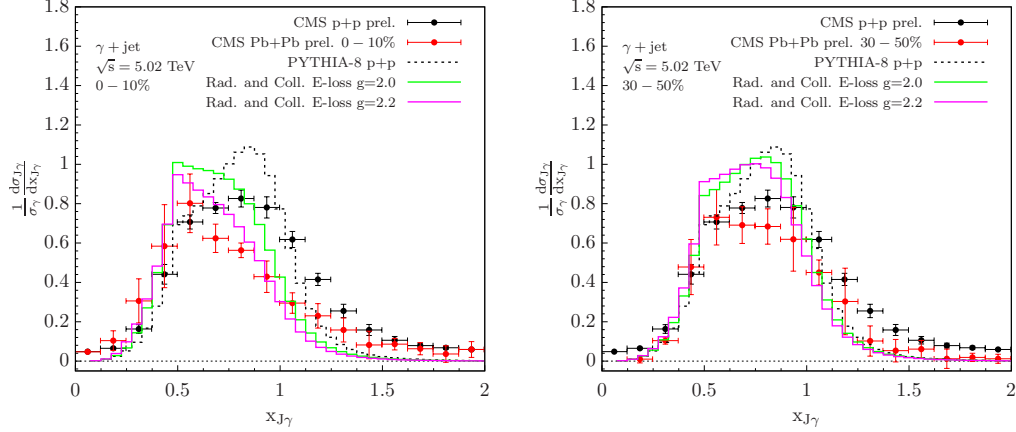


FIG. 4. The isolated photon-tagged jet asymmetry distributions are shown and compared to CMS data in central (left) and semi-central (right) collisions [25]. The transverse momenta for the isolated photon and the jet are $p_T^\gamma > 60$ GeV and $p_T^J > 30$ GeV, respectively. The jet radius parameter is $R = 0.3$. The p+p baseline, simulated by Pythia 8, is shown in the black dashed line. The theoretical results for Pb+Pb collisions with two different jet-medium coupling strengths are shown by green ($g = 2.0$) and magenta ($g = 2.2$) lines.

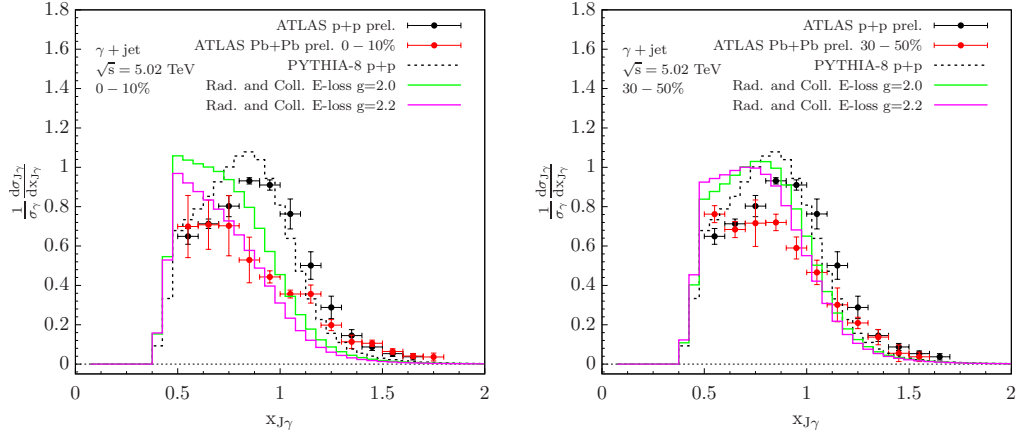


FIG. 5. Same as in Fig. 4, but for comparison to ATLAS data with jet radius $R = 0.4$ [26].

different cuts on p_T^γ . We see similar behavior in the $x_{J\gamma}$ distribution for isolated γ +jet production as in the x_{JZ} distribution for Z^0 +jet production. This is expected, as both processes are dominated by Compton scattering, which leads to similar energy loss effects.

Another classical observable to quantify nuclear modification effects in V+jet systems is I_{AA} , which is defined as ratio of the tagged differential cross section in A+A collisions to the binary collision scaled p+p result,

$$I_{AA} = \frac{1}{\langle N_{\text{bin}} \rangle} \frac{d\sigma^{AA}}{[p_T^V] dp_T^J} \bigg/ \frac{d\sigma^{pp}}{[p_T^V] dp_T^J}, \quad (12)$$

TABLE II. Theoretical results for the difference of averaged $x_{J\gamma}$ between p+p and Pb+Pb central collisions (0 – 30%). The center-of-mass energy is $\sqrt{s} = 5.02$ TeV, the transverse momentum cuts for the recoil jet is $p_T^J > 30$ GeV.

p_T^γ (GeV)	$\Delta\langle x_{J\gamma} \rangle$				
	40 – 50	50 – 60	60 – 80	80 – 100	100 – 120
CMS prel. [25]	0.008 ± 0.074	0.043 ± 0.069	0.081 ± 0.059	0.054 ± 0.044	0.115 ± 0.047
Rad. + Coll. $g = 2.0$	0.021	0.044	0.065	0.075	0.065
Rad. + Coll. $g = 2.2$	0.025	0.055	0.085	0.103	0.115

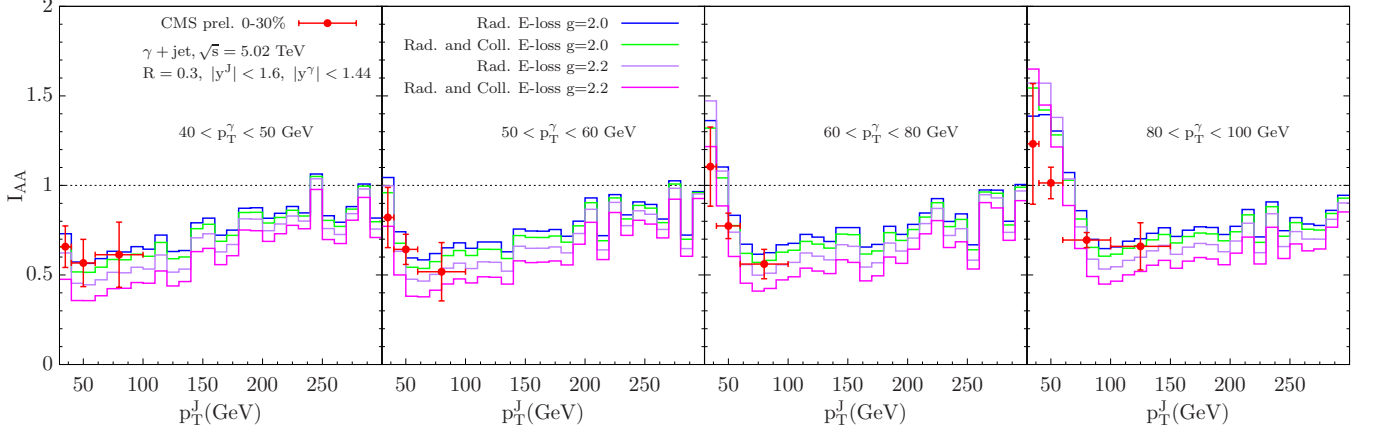


FIG. 6. The transverse momentum cuts dependence of I_{AA} are shown comparing to CMS data. We have chosen four different setups of energy loss effects: with and without collisional energy loss for both $g = 2.0$ and $g = 2.2$.

where $\langle N_{\text{bin}} \rangle$ is the average number of binary nucleon-nucleon collisions for a given centrality. In this notation we imply that the transverse momentum of the vector boson is integrated in the appropriate range

$$\frac{d\sigma}{[p_T^V]dp_T^J} \equiv \int_{p_T^{V,\min}}^{p_T^{V,\max}} \frac{d\sigma}{dp_T^V dp_T^J} \cdot \quad (13)$$

Our theoretical calculations for I_{AA} in isolated γ +jet production in 0 – 30% Pb+Pb collisions are shown in Fig. 6, and compared to CMS experimental data. We find that our results agree with data for a wide kinematic range. In each p_T^γ window, the energy loss effects are shown in four curves with different colors, which correspond to a combination of two different jet-medium coupling strength, $g = 2.0$ and $g = 2.2$, as well as the situations where we either include or exclude the collisional energy loss effects in our calculations. As one has expected, the energy loss effect is more pronounced when we include collisional energy loss and a larger jet-medium coupling strength. One can see clearly in Fig. 6 that there is a sensitive kinematical dependence of I_{AA} . The largest suppression is observed along the diagonal region of the transverse momenta of the trigger γ and the recoil jet: $p_T^\gamma \approx p_T^J$. This arises from the steeper falling cross section in the transverse momenta diagonal region. As we expect, the cross section in the region $p_T^J > p_T^\gamma$ is suppressed, and enhanced in $p_T^J < p_T^\gamma$. This is characteristic of in-medium tagged-jet dynamics. We further present theoretical predictions on the nuclear modification factor I_{AA} for Z^0 +jet in Fig. 7, which show similar p_T^Z and p_T^J dependence as those observed in γ +jet process.

Taking into account the observables that we have investigated, the x_{JV} momentum imbalance distributions, the mean x_{JV} shift, and the tagged jet modification I_{AA} we find that data favors coupling strengths between the jet and the medium in the range $g = 2.0$ to $g = 2.2$ (corresponding to $\alpha_s = 0.32$ to $\alpha_s = 0.39$ at tree level). While the asymmetry distributions prefer the larger values of the coupling strength g , the I_{AA} distributions prefer smaller values of g . Due to the complexity of the physics involved in heavy ion collisions, every theoretical calculation is bound to have model dependence. However, the amount of out-of-cone energy redistribution due to radiative and collisional processes needed for modification comparable to experimental measurements is relatively robust since it only depends on the differential transverse momentum distribution of the recoiling jet and the proper inclusion of the Jacobian factor that accounts for the energy loss in Eq. (1). We present in Table III the results for the mean out-of-cone energy loss of prompt quark-initiated and prompt gluon-initiated 100 GeV jets of small radius $R = 0.3$ in central 0-10%

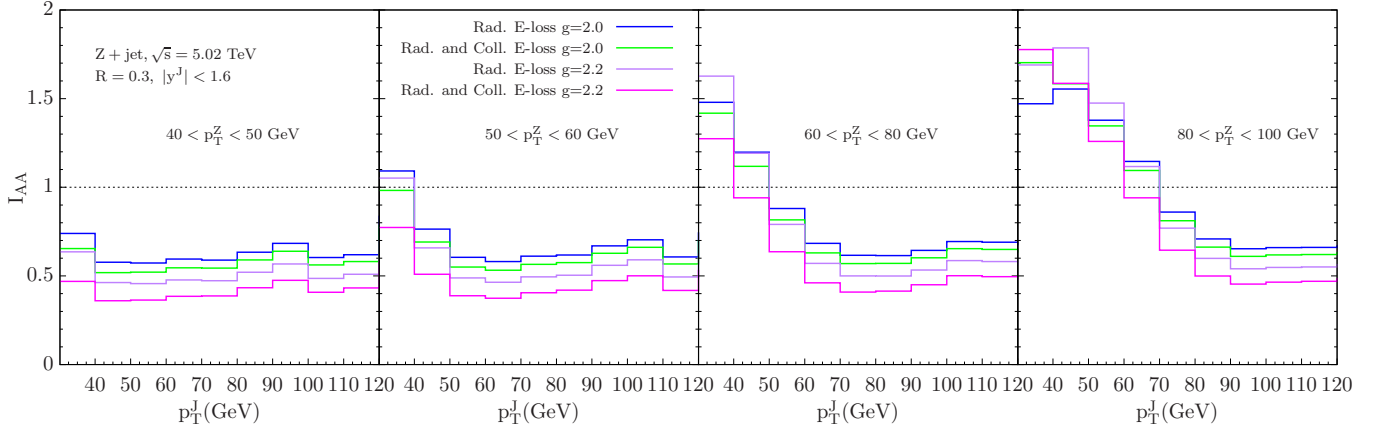


FIG. 7. The predicted transverse momentum cuts dependence of I_{AA} for Z^0 +jet in central (0 – 30%) Pb+Pb collisions at $\sqrt{s_{NN}} = 5.02$ TeV. The jet radius parameter is $R = 0.3$.

TABLE III. The mean energy loss for 100 GeV jets of $R = 0.3$ initiated by prompt quarks and gluons rounded to the nearest GeV. Central 0 – 10% Pb+Pb collisions at $\sqrt{s_{NN}} = 5.02$ TeV are considered.

	$\langle \Delta E_{q,g}^{\text{out}} \rangle = E_{q,g}^{\text{jet}} \langle \epsilon \rangle f_{q,g}^{\text{loss}}(R)$			
Type of E-loss	Rad. $g=2.0$	Rad.+Col. $g=2.0$	Rad. $g=2.2$	Rad.+Col. $g=2.2$
Prompt quark-initiated jet	7 GeV	8 GeV	10 GeV	14 GeV
Prompt gluon-initiated jet	15 GeV	18 GeV	21 GeV	29 GeV

Pb+Pb collisions at $\sqrt{s_{NN}} = 5.02$ TeV. One caveat that we must point out is that these numbers represent the upper limits. The reason for that is that multi-gluon fluctuations lead to effective energy losses smaller than the mean. We find that radiative energy losses dominate, however collisional energy loss can be as large as 40% correction to the radiative energy loss. This effect arises from the high gluon multiplicity in the medium-induced parton shower, which amplifies collisional energy losses. This can be clearly seen by comparing the two different couplings g between the jet and the medium. The fractional growth of the out-of-cone radiation when we include collisional energy loss is larger for $g = 2.2$ in comparison to $g = 2.0$ because the multiplicity of the medium-induced parton shower is larger in addition to the collisional energy loss for each individual gluon being larger itself. Last but not least, by comparing the magnitudes of out-of-cone energy loss for different scenarios we see that the strength of nuclear modification of the observables indeed follows the ordering of $\langle \Delta E_{q,g}^{\text{out}} \rangle$.

V. CONCLUSIONS

In summary, in this paper we presented a new study of vector boson-tagged (either isolated γ or Z^0) jet production in Pb+Pb collisions at a center-of-mass energy per nucleon pair of 5.02 TeV. This work is timely since new experimental results on these final states from the LHC experiments are becoming available. Within the traditional energy loss approach, by including both collisional and radiative energy loss effects, we evaluated several experimentally relevant observables: the so-called transverse momentum imbalance x_{JV} distribution modification in going from p+p to Pb+Pb collisions, the related mean momentum imbalance shift $\Delta \langle x_{JV} \rangle$, and the tagged jet nuclear modification factor I_{AA} . While some tension remains between the baseline Pythia simulations and the experimental measurements, which at present are not unfolded for detector resolution effects, we found good agreement between the theoretical simulations of the modification of these observables for coupling strengths between the jet and the medium $g = 2.0$ to $g = 2.2$ and the experimental results. This agreement is encouraging, and supports the emerging picture of the in-medium parton shower formation as encoded in these calculations. Both γ -tagged and Z^0 -tagged jets are very effective in selecting prompt quark-initiated jets and can provide valuable information on the flavor dependence of parton energy loss. We further found that while for small radius jets radiative energy loss gives the dominant contribution, collisional energy loss may play a significant role, especially for larger coupling strengths of the interaction between the jet and the medium. We conclude by emphasizing that the substructure modification of γ -tagged and Z^0 -tagged jets can differ

quite substantially from the substructure modification of inclusive jets and future experimental measurements of such observables can add significantly to our understanding of in-medium QCD dynamics.

ACKNOWLEDGMENTS

We thank Yen-Jie Lee, Qiuguang Liu, Dennis V. Perepelitsa and Kaya Tatar for helpful discussions and suggestions. This work is supported by the U.S. Department of Energy under Contract Nos. DE-AC52-06NA25396 (Z.K., I.V.), DE-FG02-91ER40684 (H.X.), and DE-AC02-06CH11357 (H.X.).

-
- [1] ATLAS, G. Aad *et al.*, JHEP **07**, 032 (2013), arXiv:1304.7098.
 - [2] ATLAS, G. Aad *et al.*, Phys. Rev. **D89**, 052004 (2014), arXiv:1311.1440.
 - [3] ATLAS, M. Aaboud *et al.*, (2016), arXiv:1611.06586.
 - [4] CMS, S. Chatrchyan *et al.*, JHEP **06**, 009 (2014), arXiv:1311.6141.
 - [5] CMS, S. Chatrchyan *et al.*, Phys. Rev. **D88**, 112009 (2013), arXiv:1310.3082.
 - [6] CMS, V. Khachatryan *et al.*, Phys. Rev. **D91**, 052008 (2015), arXiv:1408.3104.
 - [7] CMS, V. Khachatryan *et al.*, JHEP **10**, 128 (2015), arXiv:1505.06520, [Erratum: JHEP04,010(2016)].
 - [8] S. Catani, M. Fontannaz, J. P. Guillet, and E. Pilon, JHEP **05**, 028 (2002), arXiv:hep-ph/0204023.
 - [9] R. Boughezal *et al.*, Phys. Rev. Lett. **116**, 152001 (2016), arXiv:1512.01291.
 - [10] A. Gehrmann-De Ridder, T. Gehrmann, E. W. N. Glover, A. Huss, and T. A. Morgan, Phys. Rev. Lett. **117**, 022001 (2016), arXiv:1507.02850.
 - [11] ATLAS, G. Aad *et al.*, Phys. Rev. Lett. **110**, 022301 (2013), arXiv:1210.6486.
 - [12] ATLAS, G. Aad *et al.*, Phys. Rev. **C93**, 034914 (2016), arXiv:1506.08552.
 - [13] CMS, S. Chatrchyan *et al.*, JHEP **03**, 022 (2015), arXiv:1410.4825.
 - [14] D. K. Srivastava, C. Gale, and T. C. Awes, Phys. Rev. **C67**, 054904 (2003), arXiv:nucl-th/0212081.
 - [15] W. Dai, I. Vitev, and B.-W. Zhang, Phys. Rev. Lett. **110**, 142001 (2013), arXiv:1207.5177.
 - [16] E. L. Berger, J. Gao, Z.-B. Kang, J.-W. Qiu, and H. Zhang, Phys. Rev. **D91**, 113001 (2015), arXiv:1503.08836.
 - [17] R. B. Neufeld, I. Vitev, and B. W. Zhang, Phys. Rev. **C83**, 034902 (2011), arXiv:1006.2389.
 - [18] R. B. Neufeld and I. Vitev, Phys. Rev. Lett. **108**, 242001 (2012), arXiv:1202.5556.
 - [19] X.-N. Wang and Y. Zhu, Phys. Rev. Lett. **111**, 062301 (2013), arXiv:1302.5874.
 - [20] R. Kunnawalkam Elayavalli and K. C. Zapp, Eur. Phys. J. **C76**, 695 (2016), arXiv:1608.03099.
 - [21] J. Casalderrey-Solana, D. C. Gulhan, J. G. Milhano, D. Pablos, and K. Rajagopal, JHEP **03**, 053 (2016), arXiv:1508.00815.
 - [22] J. Huang, Z.-B. Kang, I. Vitev, and H. Xing, Phys. Lett. **B750**, 287 (2015), arXiv:1505.03517.
 - [23] Y.-T. Chien and I. Vitev, JHEP **05**, 023 (2016), arXiv:1509.07257.
 - [24] CMS, A. M. Sirunyan *et al.*, (2017), arXiv:1702.01060.
 - [25] CMS, C. Collaboration, (2016).
 - [26] ATLAS, T. A. collaboration, (2016).
 - [27] T. Sjostrand, S. Mrenna, and P. Z. Skands, Comput. Phys. Commun. **178**, 852 (2008), arXiv:0710.3820.
 - [28] J. Pumplin *et al.*, JHEP **07**, 012 (2002), arXiv:hep-ph/0201195.
 - [29] M. Cacciari, G. P. Salam, and G. Soyez, JHEP **04**, 063 (2008), arXiv:0802.1189.
 - [30] CMS, C. Collaboration, (2016).
 - [31] B. G. Zakharov, JETP Lett. **65**, 615 (1997), arXiv:hep-ph/9704255.
 - [32] R. Baier, Y. L. Dokshitzer, A. H. Mueller, S. Peigne, and D. Schiff, Nucl. Phys. **B483**, 291 (1997), arXiv:hep-ph/9607355.
 - [33] M. Gyulassy, P. Levai, and I. Vitev, Phys.Rev.Lett. **85**, 5535 (2000), arXiv:nucl-th/0005032.
 - [34] U. A. Wiedemann, Nucl. Phys. **B588**, 303 (2000), arXiv:hep-ph/0005129.
 - [35] X.-N. Wang and X.-f. Guo, Nucl. Phys. **A696**, 788 (2001), arXiv:hep-ph/0102230.
 - [36] P. B. Arnold, G. D. Moore, and L. G. Yaffe, JHEP **06**, 030 (2002), arXiv:hep-ph/0204343.
 - [37] G. Ovanessian and I. Vitev, Phys.Lett. **B706**, 371 (2012), arXiv:1109.5619.
 - [38] G. Ovanessian, F. Ringer, and I. Vitev, Phys. Lett. **B760**, 706 (2016), arXiv:1512.00006.
 - [39] E. Braaten and M. H. Thoma, Phys. Rev. **D44**, R2625 (1991).
 - [40] S. Wicks, W. Horowitz, M. Djordjevic, and M. Gyulassy, Nucl. Phys. **A784**, 426 (2007), arXiv:nucl-th/0512076.
 - [41] A. Adil, M. Gyulassy, W. A. Horowitz, and S. Wicks, Phys. Rev. **C75**, 044906 (2007), arXiv:nucl-th/0606010.
 - [42] M. H. Thoma, Rev. Mod. Phys. **81**, 959 (2009), arXiv:0801.0956.
 - [43] H. Berrehrah *et al.*, Phys. Rev. **C89**, 054901 (2014), arXiv:1308.5148.
 - [44] R. B. Neufeld, I. Vitev, and H. Xing, Phys. Rev. **D89**, 096003 (2014), arXiv:1401.5101.
 - [45] Y.-T. Chien and I. Vitev, (2016), arXiv:1608.07283.
 - [46] Z.-B. Kang, F. Ringer, and I. Vitev, (2017), arXiv:1701.05839.
 - [47] I. Vitev, S. Wicks, and B.-W. Zhang, JHEP **11**, 093 (2008), arXiv:0810.2807.
 - [48] R. B. Neufeld and I. Vitev, Phys. Rev. **C86**, 024905 (2012), arXiv:1105.2067.

- [49] Y.-T. Chien, A. Emerman, Z.-B. Kang, G. Ovanessian, and I. Vitev, Phys. Rev. **D93**, 074030 (2016), arXiv:1509.02936.
- [50] Z.-B. Kang, R. Lashof-Regas, G. Ovanessian, P. Saad, and I. Vitev, Phys. Rev. Lett. **114**, 092002 (2015), arXiv:1405.2612.
- [51] Z.-B. Kang, F. Ringer, and I. Vitev, (2016), arXiv:1610.02043.